Rhodopsin Photointermediates in Two-Dimensional Crystals at Physiological Temperatures †

ARTICLE *in* BIOCHEMISTRY · MAY 2006

Impact Factor: 3.02 · DOI: 10.1021/bi0524619 · Source: PubMed

Published in final edited form as:
Biochemistry. 2006 April 18; 45(15): 4974–4982. doi:10.1021/bi0524619.

Rhodopsin Photointermediates in 2D Crystals at Physiological Temperatures

Istvan Szundi[‡], **Jonathan J. Ruprecht**[§], **Jacqueline Epps**[‡], **Claudio Villa**[§], **Trevor E. Swartz**[‡], **James W. Lewis**[‡], **Gebhard F.X. Schertler**[§,**], and **David S. Kliger**[‡,*]
Department of Chemistry and Biochemistry, University of California, Santa Cruz, Santa Cruz, California 95064, USA. MRC Laboratory of Molecular Biology, Cambridge, UK

Abstract

Bovine rhodopsin photointermediates formed in 2D rhodopsin crystal suspensions were studied by measuring the time dependent absorbance changes produced after excitation with 7 nanosecond laser pulses at 15, 25 and 35 °C. The crystalline environment favored the Meta I_{480} photointermediate, with its formation from Lumi beginning faster than it does in rhodopsin membrane suspensions at 35 °C and its decay to a 380 nm absorbing species being less complete than it is in the native membrane at all temperatures. Measurements performed at pH 5.5 in 2D crystals showed that the 380 nm absorbing product of Meta I_{480} decay did not display the anomalous pH dependence characteristic of classical Meta II in the native disk membrane. Crystal suspensions bleached at 35 °C and quenched to 19 °C showed that a rapid equilibrium existed on the ~1 second time scale which suggests that the unprotonated predecessor of Meta II in the native membrane environment (sometimes called MII_a), forms in 2D rhodopsin crystals, but that the non-Schiff base proton uptake completing classical Meta II formation is blocked there. Thus, the 380 nm absorbance arises from an on-pathway intermediate in GPCR activation and does not result from early Schiff base hydrolysis. Kinetic modeling of the time-resolved absorbance data of the 2D crystals was generally consistent with such a mechanism, but details of kinetic spectral changes and the fact that the residuals of exponential fits were not as good as are obtained for rhodopsin in the native membrane suggested the photoexcited samples were heterogeneous. Variable fractional bleach due to the random orientation of linearly dichroic crystals relative to the linearly polarized laser was explored as a cause of heterogeneity but was found unlikely to fully account for it. The fact that the 380 nm product of photoexcitation of rhodopsin 2D crystals is on the physiological pathway of receptor activation suggests that determination of its structure would be of interest.

Rhodopsin, the visual pigment used in dim light, originally attracted attention as the majority photoreceptor protein in mammalian retinas, with study of the intermediates in its photoactivation sequence starting long before its function as a G protein-coupled receptor (GPCR) was revealed (1). In virtually all other GPCRs the study of activation intermediates is extremely difficult because the diffusional nature of chemoreception does not allow the rapid triggering required for early intermediate characterization using ensemble based methods. While progress has been made in detecting intermediates in chemoreceptor GPCRs (2-4), it is only with great effort that processes 10,000 times slower than those reported here are studied.

** Alternate corresponding author: MRC Laboratory of Molecular Biology, Cambridge CB2 2QH UK, Telephone: 0044 1223 402328, email: gfx@mrc-lmb.cam.ac.uk.
* Department of Chemistry and Biochemistry, University of California, Santa Cruz, CA 95064 USA Telephone: (831) 459−2106, FAX: (831) 459−2935, email: kliger@chemistry.ucsc.edu
‡ University of California, Santa Cruz.
§ MRC Laboratory of Molecular Biology.

The detailed structural information available for the inactive, dark state of rhodopsin (5,6) provides an unambiguous basis for structural modeling of the earliest photointermediates. Optical methods of detection, such as time-resolved absorbance measurements (7), provide the highest time resolution of any experimental technique and thus can be used to study a sequence of photointermediates under physiological conditions (shown in Figure 1) that connects most directly to the dark state, but the structural content is limited to specific aspects of the chromophore monitored. It is fortunate therefore that some of the photointermediates can be thermally trapped in a form that could be characterized structurally using electron cryomicroscopy. The first rhodopsin photointermediate to be trapped in a form that could be characterized in more detail by electron crystallography was metarhodopsin I, whose structure was determined under appropriate conditions in 2-dimensional crystals (8). However, the relationship of thermally trapped intermediates to those seen under physiological conditions is by no means simple and can be even more complex in a perturbed membrane environment such as exists in 2D rhodopsin crystals. Thus time-resolved measurements performed directly on rhodopsin crystals are of interest in order to clarify the relationship of the trapped photointermediate to those that appear physiologically. This is particularly important in the case of metarhodopsin I in 2D crystals because, on warming, the subsequent intermediate lacks important characteristics of metarhodopsin II (9-11), the intermediate normally produced from metarhodopsin I in the native rhodopsin membrane. A goal of the time-resolved absorbance measurements on suspensions of rhodopsin crystals reported here was to determine the relationship of the photointermediates in those crystals to the normal bleaching sequence that appears after photoexcitation of more commonly studied preparations such as rhodopsin in membrane or detergent suspensions.

MATERIALS AND METHODS

Preparation of rhodopsin crystal suspensions for optical measurements

Bovine rhodopsin crystal suspensions (see Figure 2) were prepared in dialysis buffer (20 mM Hepes, 100 mM NaCl, 10 mM $MgCl_2$, 3 mM NaN_3, 4 mM mercaptoethanol, 4 mM dithiothreitol, 2.5% v/v isopropanol adjusted to pH 7) as described previously (12,13). Rhodopsin crystal samples in dialysis buffer showed high turbidity, presumably due to crystal aggregation caused by the relatively high ionic strength of that buffer. Further, the results of preliminary time-resolved optical measurements suggested that significant settling of aggregates took place in the barrel of the syringe pump used for sample delivery during the 45 minute course of a typical experiment. To reduce both these problems, for the measurements reported here rhodopsin crystal samples were spun down (15K rpm, 20 minutes, Sorvall SS-34) and resuspended in low salt TRIS buffer (10 mM TRIS, 2 mM $MgCl_2$, 0.1 mM EDTA) at pH 7 or low salt MES buffer (10 mM MES, 2 mM $MgCl_2$, 0.1 mM EDTA) at pH 5.5 to produce a concentration of approximately 0.7 mg/mL rhodopsin. Time-resolved absorption experiments in low salt buffers produced similar results to those obtained in dialysis buffer, but had higher signal-to-noise ratio because of reduced light scattering. The presence of rhodopsin crystals in these low salt samples was verified by electron microscopy conducted after the experiments were finished.

Collection of time-resolved absorbance difference spectra

Individual 1 μL samples were photolyzed by 7-ns (full width at half maximum of the peak intensity) laser pulses from a dye laser, pumped by the 355-nm third harmonic of a Nd:YAG laser, that produced vertically polarized 477-nm light. The energy delivered to the sample was 80 $\mu J/mm^2$. The change in absorption spectrum at a particular time delay, ranging from 1 μs to 5.54 s after photolysis, was measured using a gated optical multichannel analyzer (7). Absorbance changes, $\Delta A_m(\lambda,t)$, were monitored at a right angle to the propagation direction of the excitation beam using a flashlamp that produced white light polarized at the magic angle,

54.7°, relative to the laser polarization direction. Absorbance measured at the magic angle is free from contributions that arise from rotational diffusion of rhodopsin rather than from absorbance changes of actual photointermediates (14). The pathlengths of the actinic light and probe light in the sample were 0.5 mm and 2.0 mm, respectively.

To investigate one possible cause of kinetic inhomogeneity seen in the above rhodopsin crystal measurements, other excitation conditions were explored. Since the two dimensional rhodopsin crystals studied here are expected to show linear dichroism, the fractional bleach of the rhodopsin within a particular crystal will vary depending on its orientation relative to the laser polarization direction. If cooperativity exists in any of the photointermediate transitions, variable fractional bleach could cause a continuous distribution of rates to appear. In order to produce a somewhat more homogeneous bleach, some crystal samples were excited by circularly polarized laser light created from the initially linearly polarized light using a Soleil-Babinet compensator set to produce 1/4 wave of retardation at 477 nm. When circularly polarized excitation was used, absorbance changes were measured at magic angle relative to the symmetry axis of excitation i.e. the laser propagation direction.

Thermal quench experiments

In order to test whether a thermally reversible equilibrium existed on the time scale of seconds after excitation of rhodopsin crystal suspensions, we compared absorbance spectra of samples excited at 35 °C and measured ~1 seconds later either at 35 °C or after quenching to 19 °C. To do this a 300 μL sample of rhodopsin suspension was equilibrated at 35 °C in a 0.25 mL glass tuberculin syringe. The syringe was completely surrounded by the reflectors of three photoflash units (whose light was filtered with Schott OG530 colored glass) which were triggered sequentially at 100 ms intervals, after which the contents of the syringe were injected within 1 second into 1.2 mL of stirred low salt TRIS buffer equilibrated at either 35 °C or 15 °C in a 1 cm pathlength cuvette. Spectra were recorded with a Hewlett Packard 8452A diode array spectrophotometer within 3 seconds.

Analysis of time-resolved spectra

The set of experimental magic angle difference spectra, $\{\Delta A_m(\lambda,t)\}$, were analyzed by singular value decomposition (SVD) and global exponential fitting (15). In SVD the data matrix, $\Delta\mathbf{A}$, is split into a product of three matrices: $\Delta\mathbf{A} = \mathbf{U}*\mathbf{S}*\mathbf{V}'$, where **U** is a matrix of orthogonal spectral vectors, **V** is their time dependence, and **S** contains the significance values indicative of the contributions of the **U** and **V** vectors to the experimental data. The significant vectors in the temporal matrix, **V**, are fitted to a sum of exponential functions followed by calculation of the spectral amplitudes, the b-spectra. From the b-spectra and exponential functions the matrix of reproduced data, $\Delta\mathbf{a}$, is calculated:

$$\Delta a(\lambda,t) \equiv b_0(\lambda) + b_1(\lambda)\exp(-t/\tau_1) + b_2(\lambda)\exp(-t/\tau_2) + \ldots$$

where the τ_i are the apparent lifetimes and the $b_i(\lambda)$ are b-spectra corresponding to difference spectra which decay with the associated lifetime. The difference between the experimental data matrix and the reproduced data, $\mathbf{R} = \Delta\mathbf{A} - \Delta\mathbf{a}$, gives the matrix of residuals that is used to judge the quality of the fit. The residual matrix of a good fit contains only spectrally featureless noise caused by the finite number of photons detected in each measurement. Equilibrium constants and, where appropriate, microscopic rate constants for specific mechanisms (for example, $k_1 \ldots k_6$ for the square scheme, see below) were determined by fitting the b-spectra using intermediate spectra as described previously (16). The amount of rhodopsin bleached by each laser pulse can be determined as described previously (17) and has been found to correlate with the amount estimated from the amplitude of the Lumi difference spectrum. Since the latter method does not suffer from the possibility of error caused by differences in light scattering, it was used here.

RESULTS

Time-resolved absorbance difference spectra collected from 1 μs to 5.54 s after photoexcitation of rhodopsin 2D crystal suspensions at temperatures 15, 25 and 35 °C are shown in Figure 3. At the earliest times the difference spectra at all temperatures are similar and have the shape typically observed when the lumirhodopsin (Lumi) photointermediate has been formed after photoexcitation of rhodopsin. As the early delay times progress, the absorbance decreases near 530 nm and increases near 460 nm as a product with the characteristics of metarhodopsin I (Meta I_{480}) is formed. At the lowest temperature, this is essentially the only process observed, but at the two higher temperatures, further formation of a 380 nm absorbing product is observed, with the most 380 nm absorbance developing in the 35 °C experiment. However, even after 5.54 seconds at 35 °C substantial amounts of Meta I_{480} remain in equilibrium with the 380 nm absorbing product, particularly compared to the essentially complete conversion to 380 nm product normally observed in membrane or detergent suspensions of rhodopsin at 35 C. In fact, the fractional conversion of Meta I_{480} to 380 nm absorbing product at 35 °C is smaller than the amount normally observed to be converted at 15 °C in membrane suspensions of rhodopsin (18), which raises the question of whether the 380 nm absorber seen in rhodopsin 2D crystal suspensions is the same one seen in membrane under these conditions. Besides the two 380 nm absorbing deprotonated Schiff base photointermediates that normally precede protonated Meta II formation in membrane, after release from lysine 296 in the rhodopsin binding pocket all-trans retinal can go on to react with other amine groups to form non-specific Schiff base products that also absorb at 380 nm.

To further characterize the 380 nm absorbing product formed in rhodopsin 2D crystal suspensions, photolysis experiments were carried out at pH 5.5 in order to determine whether the final equilibrated mixture displayed the characteristically anomalous pH dependence of the Meta I_{480} - metarhodopsin II (Meta II) reaction (19). The results of that experiment are presented in Figure 4 and show that less 380 nm absorbing product is formed as the pH is reduced, suggesting that the final product is not classical Meta II, because the hallmark of classical Meta II as originally characterized by Matthews et al. was that it has a pH dependence opposite to what would be expected for direct protonation of Schiff bases (19). Previous UV/visible absorbance studies of rhodopsin crystal suspension photoproduct formation with lower time resolution suggested that free all-trans retinal could form on the minutes time scale, and that it (through its nonspecific Schiff base products) could account for the pH dependence of the 380 nm product peak (8). If a mixture of all-trans retinal and its non-specific Schiff bases were also responsible on our faster time scale for the lack of anomalous pH dependence, the resulting equilibrium should be insensitive to rapid temperature change. However, if instead of early photoproduct decay to form all-trans retinal taking place in rhodopsin crystals, the Meta II intermediate was not fully formed there and the retinal remained bound to lysine 296, the equilibrated mixture would display rapid temperature dependence. To investigate whether the final equilibrium produced on the seconds time scale was rapidly reversible, we compared absorption spectra of samples bleached at 35 °C and measured at 35 °C to spectra of samples bleached at 35 °C, rapidly quenched to 19 °C and measured there.

Figure 5 compares the amount of 380 nm absorbance that can be converted back to 480 nm absorbance (Meta I_{480}) by dropping the temperature from 35 to 19 °C after photoexcitation of rhodopsin 2D crystals versus what is observed during a similar experiment using a membrane suspension of rhodopsin. The amplitude of the difference spectrum shown in Figure 5 for the rhodopsin 2D crystal sample clearly shows rapid reversibility of the equilibrated mixture. Even if the equilibrium mixture in the crystal sample were completely reversible thermally, the amplitude of the rhodopsin crystal difference spectrum would not be expected to be as large as the difference spectrum observed in sonicated rhodopsin membrane suspensions because the latter is considerably more forward shifted to begin with. In order to normalize the fraction

of the 380 nm product that was thermally reversible to 480 nm absorber, further experiments were conducted both in rhodopsin crystals and in membrane suspensions to measure the amount of additional 380 nm absorption normally present at 35 °C and hence to estimate the percent thermal reversibility in the thermal quenching experiment. Approximately 85% of the 380 nm absorbance in rhodopsin 2D crystal suspensions was found to be thermally reversible to a 480 nm absorber while in membrane suspensions essentially all was reversible within experimental error.

The above results suggested that early release of retinal is not a significant process on the seconds time scale, and therefore the time-resolved absorbance data for rhodopsin 2D crystal suspensions should be well described by the relatively small number of exponential components derived from the mechanism that describes rhodopsin photoexcitation products in membrane suspensions or even fewer exponentials if a subset of the membrane mechanism (i.e. no proton uptake by Meta II) prevails in rhodopsin crystals. This was found to be the case at the lower temperatures, with two exponentials providing a reasonable fit to the data at both 15 °C and 25 °C (observed lifetimes, as defined in the Methods section, of 5.9 and 160 ms, and 620 μs and 150 ms, respectively). The b-spectra associated with those fits are shown in Figure 6, and the decomposition of the b-spectra into intermediate spectra are given in Table 1. For widely separated exponential time constants, as were determined at 15 and 25 °C, the columns for the time dependent b-spectra of Table 1 give the relative fraction of each intermediate that decays (positive sign) or is formed (negative sign) in the process associated with that b-spectrum (16). For b_0, the time independent b-spectrum, the column in Table 1 gives the fraction of each intermediate predicted in the final equilibrium mixture. The data collected at 15 and 25 °C, however, do not constitute a strong test of whether a homogeneous version of the rhodopsin bleaching mechanism fully describes the crystal data because at those temperatures relatively little 380 nm absorber forms, which makes the total signal, i.e. the integrated absorbance change, fairly small.

At 35 °C larger signals were observed which allowed the data to be fit to three exponentials with lifetimes 130 μs, 4.4 and 100 ms. This fit was not entirely satisfactory because the b-spectra associated with the three processes (shown in Figure 6) were more similar in shape than the b-spectra normally seen in rhodopsin membrane suspensions, and the decomposition of the crystal b-spectra in terms of intermediate spectra (shown in Table 1) differ significantly from what would be expected from any possible variation of rates in the mechanism known to describe rhodopsin in membrane suspensions (see Appendix). Further, comparatively poor residuals were obtained from the three exponential fit, and while four exponentials produced a marginal improvement (introducing a small amplitude component with an observed lifetime of 5 seconds, describing formation of a 420 nm absorber), neither it nor fitting with more exponentials reduced the residuals to what would be expected if the sample were completely homogeneous and obeyed any possible variant of the rhodopsin mechanism as characterized in membrane. Thus, it is apparent that some sort of heterogeneity is present in the kinetics of the rhodopsin crystal sample. The significance of this is discussed below.

DISCUSSION

Complete understanding of the rhodopsin photoexcitation mechanism and the more general problem of GPCR activation requires that structures of all important intermediates that appear along the activation pathway be characterized. Achieving this goal requires both the determination of the photointermediate sequence under physiological conditions by methods with high time resolution and the application of structural tools that are likely to require non-physiological constraints. The work reported here sought to characterize the intermediates formed in rhodopsin 2D crystals, a phase which has been of great importance in rhodopsin structure determination (12) and which was used to determine the first structure of a rhodopsin

photointermediate (8). Since 2D crystals are essentially similar to the membrane phase, it is reasonable that there would be similarity in the mechanistic scheme followed in those two environments, and to a first approximation the bleaching kinetics in rhodopsin crystal suspensions can be described by a subset of the mechanism that prevails in membrane suspensions of rhodopsin (20) :

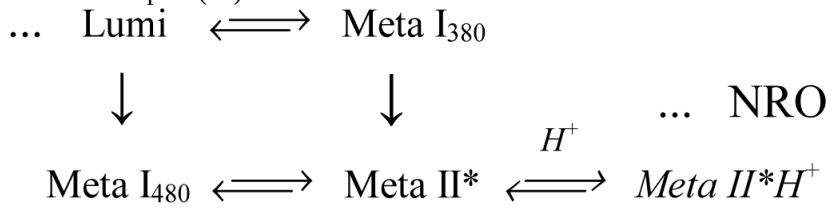

where in the mechanism above, the italicized part does not appreciably take place on the time scale studied here in crystal suspensions in the 15 − 35 °C range of temperatures, and the abbreviation NRO stands for n-retinylidene opsin, the mixture of non-specific retinal Schiff bases referred to earlier. In the scheme above Meta II*H^+ is the transducin activating species also known as R*. The absence of the final proton uptake by Meta II* in rhodopsin crystals accounts for lack of anomalous pH dependence in the final equilibrated mixture since this step was originally proposed to account for that observation (21, whose * notation for the unprotonated form of Meta II we have adopted) and has since been associated with proton uptake by glutamic acid 134 (22, note: Arnis *et al*.'s MII_a is closely related to our Meta II* as fully discussed in *23* and Arnis *et al*.'s MII_b is equivalent to our Meta II*H^+). It should be stressed that the above scheme is adopted because it has previously (20-23) been shown to describe rhodopsin under a wide range of conditions, and the major features of it seem appropriate to describe our observations in the 2D crystals.

One of the most important conclusions reached here is that the formation of 380 nm absorbance in rhodopsin crystal suspensions on the seconds time scale is primarily due to formation of Meta II*(MII_a), an intermediate of structural interest because it lies on the pathway of activation under physiological conditions. This conclusion is based on thermal quench experiments in rhodopsin crystal suspensions showing the 380 nm absorbing product to be in rapid equilibrium with its PSB precursor, Meta I_{480}. Formation of the 380 nm absorbing product from Meta I_{480}, and the fact that it does not revert to Lumi excludes the possibility that the final product is Meta I_{380}. Our assignment of the 380 nm absorbing product to Meta II*(MII_a) is also supported by FTIR measurements at 30 °C which found evidence for a species with a Meta I-like protein conformation and a deprotonated Schiff base (11) which is plausibly the FTIR signature of Meta II*(MII_a). The earlier conclusion based on UV/visible measurements (8) that on longer time scales the 380 nm absorbance is due to all-trans retinal or its non-specific Schiff base products does not conflict with the assignment here to Meta II*(MII_a) on the seconds time scale, because at 35 °C there is evidence in the kinetic results for production of a 420 nm absorber with a 5 second formation time that corresponds to the formation of the species previously characterized on the longer time scale. The 420 nm absorbance is presumably due to the protonated component of the non-specific Schiff base mixture of retinal and non-specific Schiff bases referred to as NRO reported earlier in more detail (24). This early formation of NRO was supported by measurements on the seconds to minutes time scale with the HP 8452A diode array (data not shown). This 5 second process is much faster than occurs in the native disk membrane at this temperature (24) and represents another significant kinetic difference in 2D rhodopsin crystals. Parallels exist in recombinant membrane preparations of rhodopsin where short chain, saturated lipids inhibited SB deprotonation and resulted in similar lack of anomalous pH dependence (25-27). The cause may be associated with the rigid environment in 2D crystals, analogous to the situation with detergents in the cholesteric class that similarly inhibit Schiff base deprotonation (28,29). FTIR measurements of rhodopsin reconstituted with

either distearoyl or dipalmitoyl phosphatidylcholine to form membranes showed similar behavior to measurements of 2D crystals (11).

Although the subscheme above provides a first approximation to fit the time-resolved absorption data for rhodopsin crystal suspensions, no single version of such a scheme can account for the data at 35 °C in detail. The most obvious evidence for the inadequacy of a single scheme are the poor residuals that result even when four exponentials are fit to the data, and this idea is supported by the similarity of the b-spectra shapes even when their associated lifetimes vary over three orders of magnitude in time. A less obvious, but more definitive indication of kinetic heterogeneity appears when a detailed balancing of the production and decay of the species presented in Table 1 is attempted. This analysis, presented as an appendix, shows that the unusual early production of Meta I_{480} during the process associated with b_1 and its interpretation within a single square scheme, lead to predictions which are inconsistent with the observed lifetimes and compositions of the other b-spectra. The lack of well-defined exponential processes that would be expected if a single mechanism prevails after photoexcitation of the rhodopsin crystal samples is further demonstrated by the concentration profiles shown in Figure 7. If discrete exponentials described those experiments, the concentration profiles should change over localized regions of time. However, rather than a set of plateaus separated by ramps that are characteristic of rhodopsin in membrane suspensions, the concentration profiles display more or less continuous change, varying from that only by the noise of the measurement.

In order to account for the observed kinetic data at 35 °C, a model that includes one or more additional schemes can be used to improve the fit to the concentration profiles in Figure 7. The early formation of Meta I_{480} can be accounted for by adding a parallel, single step scheme that incorporates a fast Lumi decay concurrent with the primary membrane scheme. This additional fast scheme only needs a single step since large amounts of Meta I_{480} do not decay further on the time scale of the measuements here. However, besides the fast scheme, a further additional parallel scheme is required in order to account for the spectral changes occurring at least an order of magnitude slower than what is observed in rhodopsin membrane suspensions at 35 ° C. This slow scheme has all the steps typically seen in membrane (except proton uptake), but has microscopic rates 1 to 2 orders of magnitude slower than what prevails in membrane. The rate constants obtained for the three schemes required to fit the rhodopsin crystal data are given in Table 2, and the fit to the concentration profiles are shown in Figure 7. The largest fraction of the sample follows a scheme similar to rhodopsin in membrane suspension, but the rate constants are somewhat slower than seen there. Modeling of the 35 °C rhodopsin crystal suspension data in terms of three parallel schemes was performed in order to demonstrate that the data can be fit with a limited number of processes and to show the characteristics of the data in a concrete form. The exact details of the model are not unique and should not be taken to necessarily imply that three populations of rhodopsin are present or that an alternative representation in terms of stretched exponentials is excluded, but rather should taken to indicate the degree to which the data for rhodopsin crystal suspensions are incompatible with a homogeneous kinetic model.

Kinetic heterogeneity in rhodopsin crystal suspensions has several possible origins. One possible cause is the physical heterogeneity apparent when the samples are examined using low magnification electron microscopy after negative staining with 1% uranyl acetate (12). Besides the tubular $p22_12_1$ crystals, some single layers are present as well as small areas of denser staining material. Efforts were made to enrich samples in well-formed crystals using sucrose density gradients, but this did not materially reduce the apparent kinetic heterogeneity compared to the fractions containing more non-crystalline forms. However, even if all the particles in the sample were identical a number of other causes of heterogeneity are possible. One example involves the topology of the $p22_12_1$ crystals, where environmental heterogeneity

could exist for rhodopsins located in different parts of a particular crystal. Because $p22_12_1$ forms tubular or monolayer crystals there will potentially be edge effects. This unusual feature of $p22_12_1$ crystals has no direct analog in studies of rhodopsin in membrane vesicle suspensions, which provide a homogeneous rhodopsin environment making it difficult to assess. However, rhodopsin's bleaching kinetics in different recombinant membrane preparation show it to be sensitive to its membrane environment (26,27,30,31), potentially causing the kinetics of a particular rhodopsin to depend on its proximity to a crystal edge.

Besides the heterogeneity due to preexisting factors discussed above, pulsed excitation with a linearly polarized laser creates an orientationally dependent heterogeneity because $p22_12_1$ crystals are dichroic. On the time scale of the 7 ns excitation pulse used here, crystals are completely static so that the fractional bleach of all rhodopsins in a particular crystal will be highest for crystals whose long axis is aligned with the linear polarization axis of the exciting light. Secondary excitation of photoproducts will also be highest in those crystals. Rhodopsin is known to undergo a significant volume change on formation of the metarhodopsin II intermediate (32), which causes the Meta I_{480} - Meta II equilibrium to be pressure dependent. Presumably this would have an effect on the kinetics of a photoexcited rhodopsin in a low fractionally bleached crystal where it is surrounded by unbleached molecules compared to the case of a more highly bleached crystal where it would have a higher probability to be surrounded by similarly excited rhodopsins. In order to assess whether this effect contributed to the kinetic heterogeneity, samples were excited with circularly polarized light. While this still does not produce a perfectly homogeneous sample (because some crystals lie with their long axis along the propagation direction of the exciting light) it essentially reverses the bias in the fractional bleaching distribution from relatively low fractional bleach to relatively high fractional bleach. For circularly polarized excitation the minority of crystals (i.e. those whose long axis lies in the polar regions relative to the symmetry axis defined by the propagation direction) are the population with lower fractional bleach. The results of the circularly polarized excitation experiments showed a small increase in amplitude of the slowest component detected, but the increase was of marginal significance. Thus, while this effect could contribute to the heterogeneity in kinetics seen here, it seems unlikely to fully account for it.

Our characterization of the principal bleaching product in $p22_12_1$ as Meta I_{480} agrees with the conclusion of previous FTIR studies (11). Those FTIR experiments found the transition temperature for Lumi decay to be elevated by approximately 30 °C compared to what is observed for rhodopsin in membrane. The increased $p22_12_1$ Lumi stability implied by the FTIR temperature trapping experiments is consistent with our observation at 15 °C that Lumi decays in$p22_12_1$ approximately half as fast as it does in membrane suspensions (18). However, at 35 °C our measurements show the situation to be reversed and Meta I_{480} forms significantly faster in $p22_12_1$ than it does in membrane. These observations raise the possibility that some physical change takes place in the sample over the 15 − 35 °C temperature range that accelerates Lumi decay. Over the same temperature range, our measurements show a significant increase in the amount of 380 nm product formation. Previous work found the 380 nm absorbing product to be inactive toward transducin and concluded that on a longer time scale the 380 nm absorbance was accounted for by all-trans retinal and its non-specific Schiff bases (11). Here we show that on the seconds time scale the 380 nm absorbance is caused by the Meta II*(MII_a) intermediate, an on-pathway precursor of the activated form. The fraction of photoproduct appearing as Meta II*(MII_a) after a single laser pulse in a 2D crystal sample at 35 °C is approximately 0.34 as shown by the decomposition of b_0 given in Table 1, and larger amounts would be produced by a single laser pulse at higher temperatures. Further, the total production of Meta II*(MII_a) in 2D rhodopsin crystals can be substantially increased as described in the Methods section by delivering a series of orange flashes with each delayed by sufficient time that Meta II*(MII_a) forms and back photolysis is avoided. Using the prototype of this method reported here we believe that over half of the sample was converted to Meta II*(MII_a). Thus, in principal at least,

it is possible that Meta II*(MII_a), an intermediate separated from the GPCR active state by proton uptake, could be trapped in 2D crystals for structural analysis.

Acknowledgements

This work was supported by Grant EY00983 from the National Eye Institute of the National Institutes of Health (to D.S.K.), a predoctoral fellowship from MRC (to J.J.R) and the Human Frontier Science Program grant RGP52/2005 (G.F.X.S).

APPENDIX

If all the rhodopsin in a sample obeys the square scheme with a single set of microscopic rate constants, the mechanism places algebraic constraints on the shapes of the b-spectra and lifetimes that can be obtained. The purpose of this appendix is to demonstrate that the b-spectra from the three exponential fit to the data for $p22_12_1$ at 35 °C are inconsistent with those constraints.

In membrane suspensions of rhodopsin the observed lifetime of the first process is ~100 μs and the shape of the first b-spectrum at 25 and 35 °C shows it to be due to Lumi decaying while Meta I_{380} forms. Therefore, $(k_1 + k_2) >> k_3, k_4, k_5, k_6$. The first observed lifetime, t_1, is $\approx 1/(k_1 + k_2)$, and the amplitude of the first b-spectrum is approximately $k_1/(k_1 + k_2)$. The second apparent lifetime in membrane is approximately 1 ms and the shape of its b-spectrum shows decay of Lumi to both 480 and 380 nm absorbance forms, which implies that $t_2 \approx 1/(k_3 + k_4)$. The third lifetime found in membrane is approximately 10 ms and its associated b-spectrum shows Meta I_{480} decaying to Meta II, which implies $t_3 \approx 1/(k_5 + k_6)$. Thus, in membrane suspensions, the three apparent lifetimes correspond to the three levels of arrows in the square scheme (16).

In rhodopsin 2D crystal suspensions at 35 °C, the first apparent lifetime is 130 μs, but the composition of the first b-spectrum given in Table 1 shows that $k_4 > (k_1 + k_2)$. This means that the first b-spectrum is no longer confined to the process corresponding to the top row of arrows, but contains the contribution due to the left down arrow (whose associated microscopic rate is k_4). This implies that $\tau \approx 1/(k_4 + k_1 + k_2) \approx 7500\ s^{-1}$, and since a 2:1 ratio of 480 nm absorber to 380 nm absorber is formed during the process corresponding to τ_1, $k_4 \approx 2 \cdot (k_1 + k_2) \approx 5000\ s^{-1}$ and $(k_1 + k_2) \approx 2500\ s^{-1}$. The amplitude of the fast b-spectrum is still primarily determined by the top row process, so $k_1/(k_1 + k_2) \approx 0.5$ implying a balanced top equilibrium with $k_1 \approx 1250\ s^{-1}$ and $k_2 \approx 1250\ s^{-1}$. If the partial scheme constructed using these microscopic rate constants is examined, clear contradictions with the subsequent processes exist. Table 1 shows that approximately half of the Lumi initially formed decays in the second and the third processes via the two down arrows with a net production of the 380 nm absorbing form (as required by the composition of the associated b-spectra in Table 1). However, this net production requires that k_3 (associated with the right down arrow) must be larger than k_4 ($5000\ s^{-1}$), with the consequence being that all the Lumi must completely decay within 200 μs, contradicting the 4.4 ms observed second lifetime as well as the experimental b-spectra. From a qualitative standpoint, within the constraints of a single scheme, the contribution of Lumi to all three b-spectra is fundamentally incompatible with the rapid Meta I_{480} formation seen at this temperature. Thus, in addition to the other indications of heterogeneous kinetics referred to in the Discussion, as demonstrated here the b-spectra shapes and associated lifetimes are inconsistent with the data from crystal suspensions at 35 °C being described by a single scheme.

Abbreviations

GPCR, G protein-coupled receptor; HEPES, N-[2-hydroxyethylpiperazine-N'-[2-ethanesulfoninc acid]; Lumi, lumirhodopsin; MES, 2-(N-morpholino)ethanesulfonic acid;

Meta, metarhodopsin; NRO, n-retinylidene opsin; PSB, protonated Schiff base; SVD, singular value decomposition; TRIS, tris(hydroxymethyl)aminomethane.

REFERENCES

1. Kliger DS, Lewis JW. Spectral and kinetic characterization of visual pigment photointermediates. Isr. J. Chem 1995;35:289–307.
2. Vilardaga J-P, Bünemann M, Krasel C, Castro M, Lohse MJ. Measurement of the millisecond activation switch of G protein-coupled receptors in living cells. Nature Biotechnol 2003;21:807–812. [PubMed: 12808462]
3. Kobilka B. Agonist Binding: A Multistep Process. Mol. Pharmacol 2004;65:1060–1062. [PubMed: 15102933]
4. Hoffmann C, Gaietta G, Bunemann M, Adams SR, Oberdorff-Maass S, Behr B, Vilardaga JP, Tsien RY, Eisman MH, Lohse MJ. A FlAsH-based FRET approach to determine G protein - coupled receptor activation in living cells. Nature Meth 2005;2:171–176.
5. Okada T, Sugihara M, Bondar AN, Elstner M, Entel P, Buss V. The retinal conformation and its environment in rhodopsin in light of a new 2.2 angstrom crystal structure. J. Mol. Biol 2004;342:571–583. [PubMed: 15327956]
6. Li J, Edwards PC, Burghammer M, Villa C, Schertler GFX. Structure of bovine rhodopsin in a trigonal crystal form. J. Mol. Biol 2004;343:1409–1438. [PubMed: 15491621]
7. Lewis JW, Kliger DS. Absorption spectroscopy in studies of visual pigments: Spectral and kinetic characterization of intermediates. Meth. Enzymol 2000;315:164–178. [PubMed: 10736701]
8. Ruprecht JJ, Mielke T, Vogel R, Villa C, Schertler GFX. Electron crystallography reveals the structure of metarhodopsin I. EMBO J 2004;23:3609–3620. [PubMed: 15329674]
9. Beck M, Sakmar TP, Siebert F. Spectroscopic evidence for interaction between transmembrane helices 3, 4 and 5 in rhodopsin. Biochemistry 1998;37:7360–7639.
10. Vogel R, Fan GB, Siebert F, Sheves M. Anions stabilize a metarhodopsin II-like photoproduct with a protonated Schiff base. Biochemistry 2001;40:13342–13352. [PubMed: 11683644]
11. Vogel R, Ruprecht J, Villa C, Mielke T, Schertler GFX, Siebert F. Rhodopsin photoproducts in 2D crystals. J. Mol. Biol 2004;338:597–609. [PubMed: 15081816]
12. Krebs A, Villa C, Edwards PC, Schertler GFX. Characterisation of an improved two-dimensional p22121 crystal from bovine rhodopsin. J. Mol. Biol 1998;282:991–1003. [PubMed: 9753549]
13. Mielke T, Villa C, Edwards PC, Schertler GFX, Heyn MP. X-ray diffraction of heavy-atom labelled two-dimensional crystals of rhodopsin identifies the position of cysteine 140 in helix 3 and cysteine 316 in helix 8. J. Mol. Biol 2002;316:693–709. [PubMed: 11866527]
14. Lewis JW, Kliger DS. Rotational diffusion effects on absorbency measurements - limitations to the magic-angle approach. Photochem. Photobiol 1991;54:963–968. [PubMed: 1775534]
15. Hug SJ, Lewis JW, Einterz CM, Thorgeirsson TE, Kliger DS. Nanosecond photolysis of rhodopsin: evidence for a new, blue-shifted intermediate. Biochemistry 1990;29:1475–1485. [PubMed: 2334708]
16. Szundi I, Lewis JW, Kliger DS. Deriving reaction mechanisms from kinetic spectroscopy. Application to late rhodopsin intermediates. Biophys. J 1997;73:688–702. [PubMed: 9251787]
17. Albeck A, Friedman N, Ottolenghi M, Sheves M, Einterz CM, Hug SJ, Lewis JW, Kliger DS. Photolysis intermediates of the artificial visual pigment *cis*-5,6-dihydro-isorhodopsin. Biophys. J 1988;55:233. [PubMed: 2713437]
18. Thorgeirsson TE, Lewis JW, Wallace-Williams SE, Kliger DS. Effects of temperature on photointermediates from lumirhodopsin to metarhodopsin II. Biochemistry 1993;32:13861–13872. [PubMed: 8268161]
19. Matthews RG, Hubbard R, Brown PK, Wald G. Tautomeric forms of metarhodopsin. J. Gen. Physiol 1963;47:215–240. [PubMed: 14080814]
20. Jäger S, Szundi I, Lewis JW, Mah TL, Kliger DS. Effects of pH on rhodopsin photointermediates from lumirhodopsin to metarhodopsin II. Biochemistry 1998;37:6998–7005. [PubMed: 9578587]

21. Emrich HE, Reich R. Primary reactions of the visual process - Thermodynamic and kinetic influence of pH on the metarhodopsin I-II transition - Proton consumption as an effect of a conformational change. Z. Naturforsch. Teil C 1974;29:577–591. [PubMed: 4277906]
22. Arnis S, Fahmy K, Hofmann K-P, Sakmar TP. A conserved carboxylic acid group mediates light-dependent proton uptake and signaling by rhodopsin. J. Biol. Chem 1994;269:23879–23881. [PubMed: 7929034]
23. Szundi I, Mah TL, Lewis JW, Jäger S, Ernst OP, Hofmann KP, Kliger DS. Proton transfer reactions linked to rhodopsin activation. Biochemistry 1998;37:14237–14244. [PubMed: 9760262]
24. Szundi I, Lewis JW, van Kuijk FJGM, Kliger DS. Effect of NADPH on formation and decay of human metarhodopsin III at physiological temperatures. Vis. Res 2000;40:3039–3048. [PubMed: 10996607]
25. O'Brien DF, Costa LF, Ott RA. Photochemical functionality of rhodopsin - phospholipid recombinant membranes. Biochemistry 1977;16:1295. [PubMed: 557336]
26. Baldwin PA, Hubbell WL. Effects of lipid environment on the light-induced conformational-changes of rhodopsin. 1. Absence of metarhodopsin-II production in dimyristoylphosphatidylcholine recombinant membranes. Biochemistry 1985;24:2624–2632. [PubMed: 4027217]
27. Baldwin PA, Hubbell WL. Effects of lipid environment on the light-induced conformational-changes of rhodopsin. 2. Roles of lipid chain-length, unsaturation, and phase state. Biochemistry 1985;24:2633–2639. [PubMed: 4027218]
28. Schleicher A, Franke R, Hofmann KP, Finkelmann H, Welte W. Deoxylysolecithin and a new bipheny detergent as solubilizing agents for bovine rhodopsin. Functional test by formation of metarhodopsin II and binding of G-protein. Biochemistry 1987;26:5908–5916. [PubMed: 3118952]
29. Szundi I, Lewis JW, Kliger DS. Effect of digitonin on the Meta I-Meta II equilibrium. Photochem. Photobiol 2005;81:866–873. [PubMed: 15819603]
30. Mitchell DC, Straume M, Litman BJ. Role of *sn*-1-saturated,*sn*-2-polyunsaturated phospholipids in control of membrane receptor conformational equilibrium: effects of cholesterol and acyl chain unsaturation on the metarhodopsin I ⇌ metarhodopsin II equilibrium. Biochemistry 1992;31:662–670. [PubMed: 1731921]
31. Niu S-L, Mitchell DC, Litman BJ. Manipulation of cholesterol levels in rod disk membranes by methyl-β-cyclodextrin. J. Biol. Chem 2002;277:20139–20145. [PubMed: 11889130]
32. Lamola AA, Yamane T, Zipp A. Effects of detergents and high pressure upon the metarhodopsin I ⇌ metarhodopsin II equilibrium. Biochemistry 1974;13:738–745. [PubMed: 4855767]

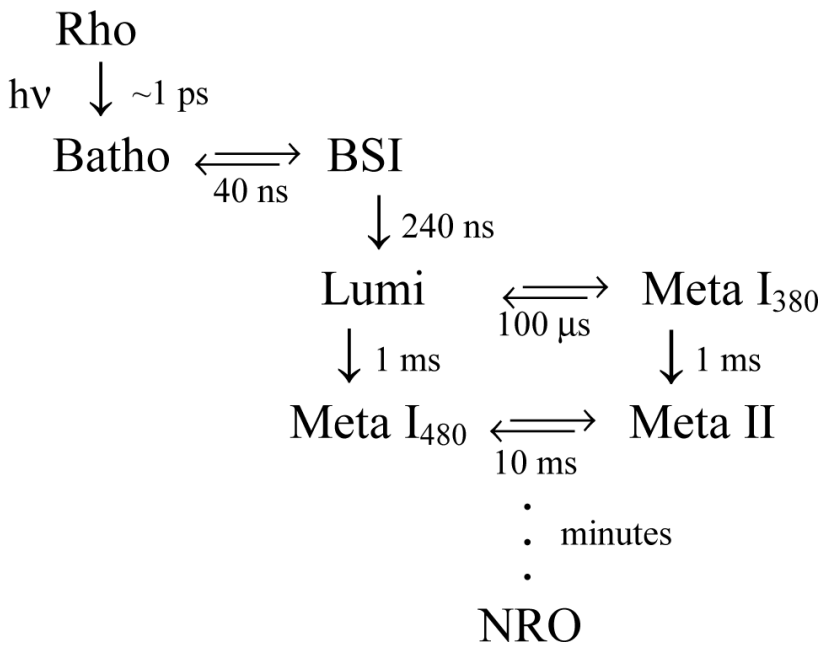

Figure 1.

Rhodopsin photointermediate scheme near physiological temperatures in membrane. Some of the above intermediates can be trapped after low-temperature photolysis, but BSI (whose equilibrated mixture with Batho is sometimes called BL) and Meta I_{380} only build up appreciable concentrations near physiological temperatures (7). The scheme shown is a simplified version describing the principal processes affecting absorbance. The time constants are appropriate for membrane suspensions of rhodopsin. This general scheme also holds for detergent samples (such as lauryl maltoside) except that beginning with Lumi, all decays are significantly faster and subsequent equilibria are more forward shifted.

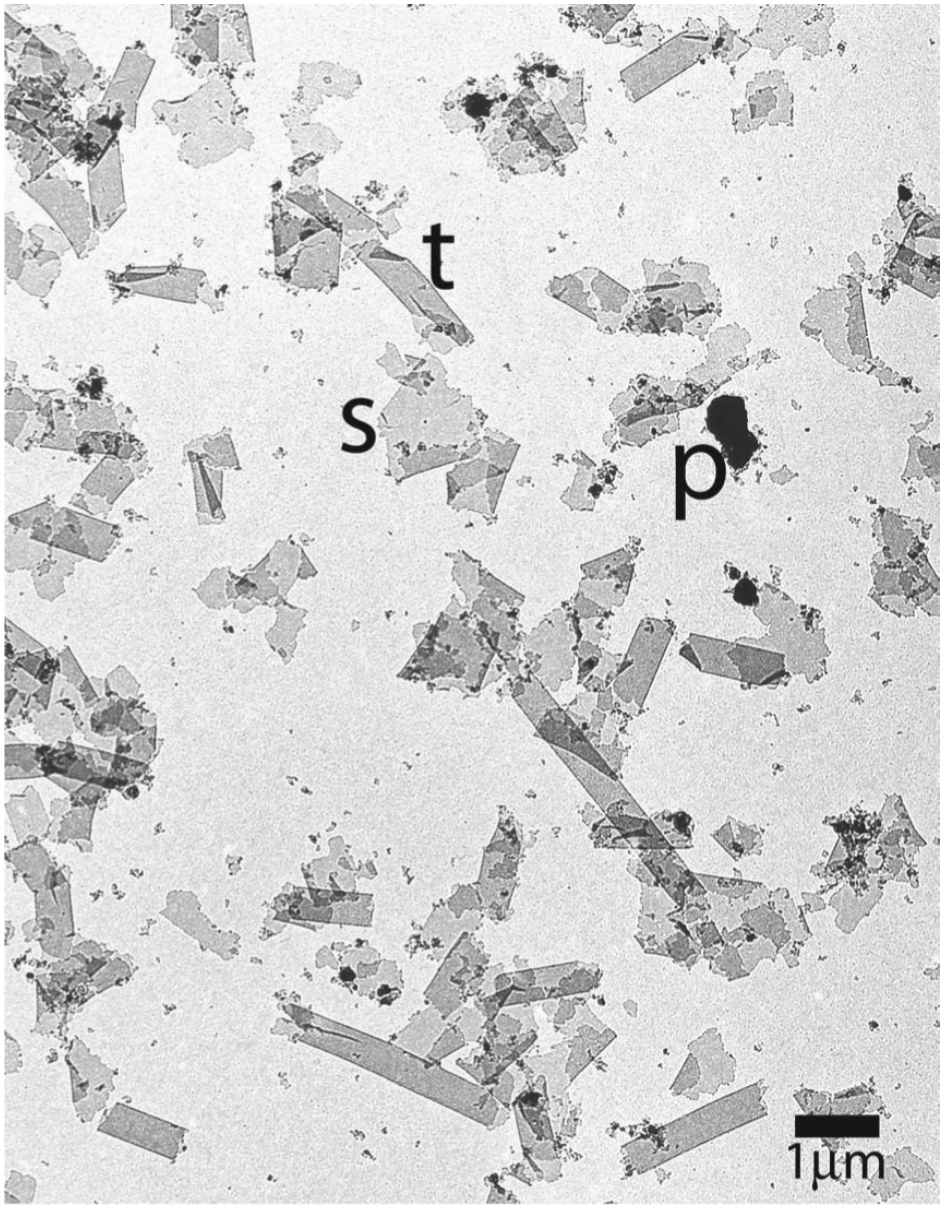

Figure 2.

Electron micrograph of 2D crystals of rhodopsin. An overview picture of a sample obtained from a dialysis reconstitution experiment was taken at low magnification and with strong defocus (300 um) to obtain high contrast. Single layer membranes (s), collapsed tubular membranes (t), and protein aggregates (p) are visible. The single layers and the tubes are two-dimensional crystals of bovine rhodopsin, which are well characterised (8,12,13). The exact nature of the protein aggregates (p) is not known.

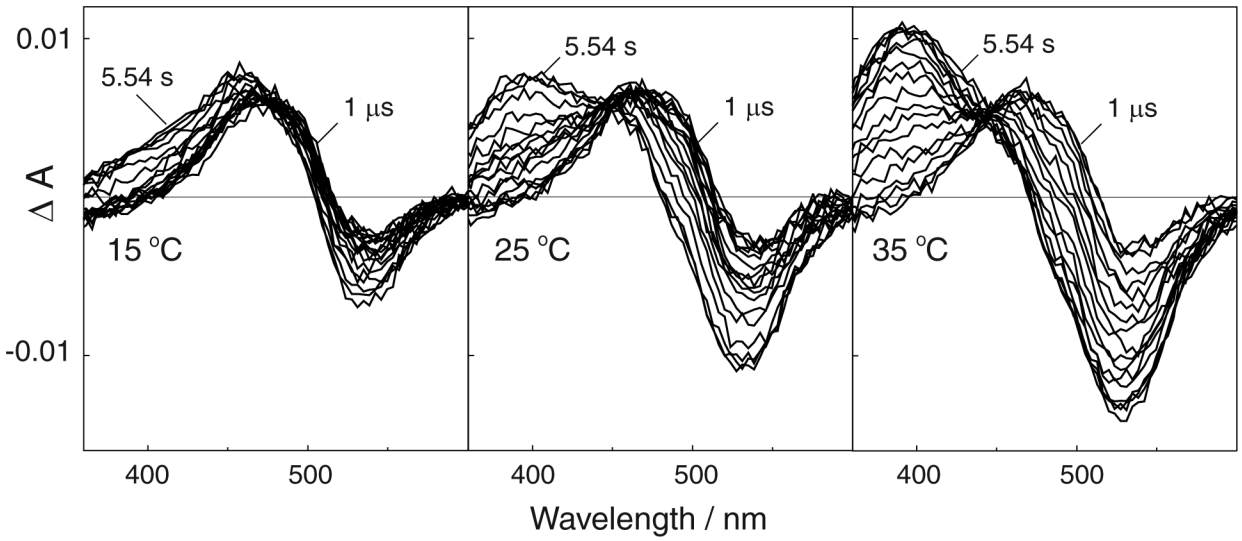

Figure 3.

Absorbance difference spectra recorded at time delays ranging from 1 μs to 5.54 s after photoexcitation of rhodopsin 2D crystal suspensions. To eliminate absorbance changes due to rotational diffusion, data were collected using probe light that was linearly polarized at the magic angle (54.7°) relative to the linear polarization direction of the 7 ns, 477 nm excitation laser pulse. Measurement temperature is shown in each panel and samples were pH 7. Although as the temperature is increased there is a substantial increase in the amount of 380 nm absorbance observed on the seconds time scale, even at 35 °C approximately 2/3 of the PSB absorbance in 2D rhodopsin crystals remains at 5.54 s after excitation. Note that the peak of the 1 μs data near 460 nm arises from the 494 nm absorbing species, Lumi, with the peak being shifted because the data reports the difference between two species (Lumi and rhodopsin) having similar λ_{max}.

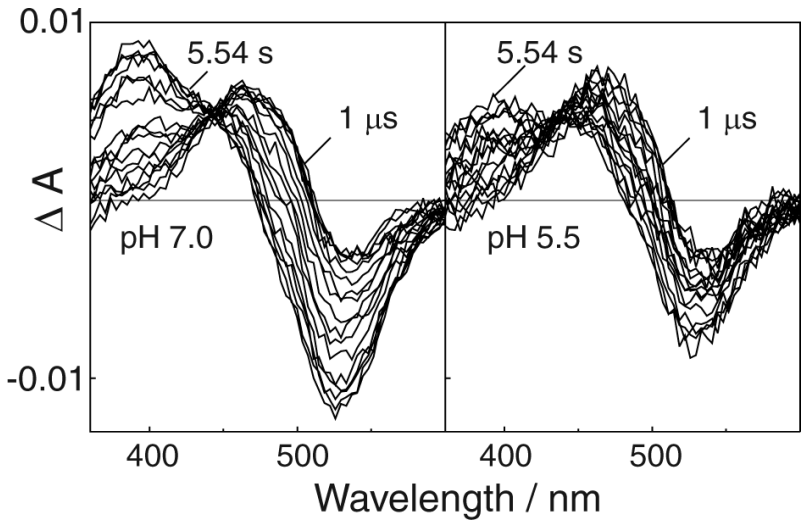

Figure 4.

pH dependence of the time-resolved absorbance difference spectra in rhodopsin 2D crystal suspensions at 35 C. Significantly less of the 380 nm absorbing species is observed on the seconds time scale in pH 5.5 low salt MES buffer compared to pH 7.0 low salt TRIS buffer. If the 380 nm absorbing product in rhodopsin 2D crystals was the “classical” Meta II photointermediate originally characterized by Matthews *et al.* (19), it should display the so-called anomalous pH dependence i.e. opposite to that expected when the Schiff base linkage titrates due to the pH change of the buffer, contrary to what is seen above. The final product in rhodopsin 2D crystals displays the usual pH dependence expected when a short wavelength absorbing Schiff base partially protonates to form the longer wavelength absorbing PSB in going from pH 7.0 to pH 5.5.

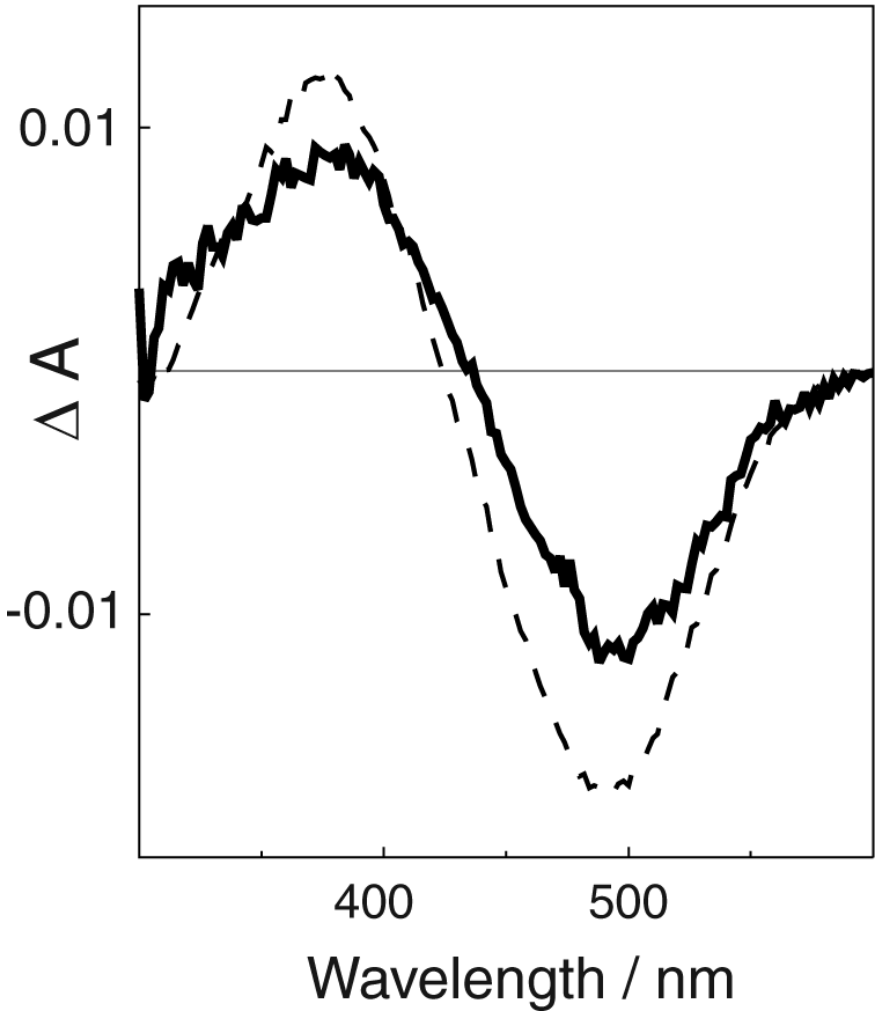

Figure 5.

Difference spectra resulting from the thermal quench of photoexcited mixtures from 35 °C to 19 °C on the seconds time scale. The solid line shows the absorbance difference between a sample of rhodopsin 2D crystal suspension that was photoexcited at 35 °C and recorded at that temperature ~1 s later and the spectrum from a sample that was similarly photoexcited at 35 °C but quenched to 19 °C before recording the spectrum. The dashed line shows the difference absorbance spectrum obtained from samples of a sonicated membrane suspension of rhodopsin in an identical experiment. To estimate the percent thermal reversibility of the equilibrium formed on the ~1 second time scale, these data need to be compared to the increase in signal recorded in constant temperature measurements over this range. Those data indicate that in membrane the equilibrium is 100% thermally reversible at ~1 s and approximately 85% thermally reversible in rhodopsin 2D crystals. Note that the larger change seen in this experiment compared to the data shown in Figure 3 for 2D rhodopsin crystals results from the larger bleach achieved by the three sequential flashes used here (see text) compared to the single laser pulses used to produce the data in Figure 3.

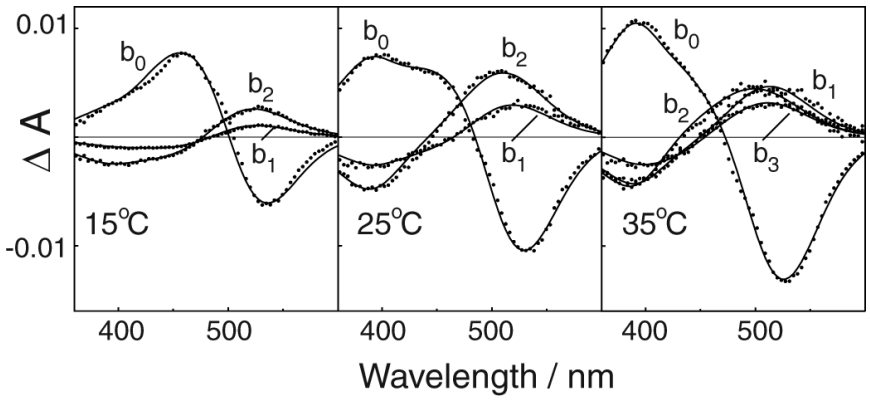

Figure 6.

Time-dependent absorbance changes (b-spectra) associated with the exponential processes that fit rhodopsin 2D crystal data. Points show the b-spectra associated with the time dependent spectral changes (two exponentials at 15 and 25 °C, and three exponentials at 35 °C) and with b_0, the time independent absorbance change due to excitation. Curves show the fit to the b-spectra obtained using the photointermediate compositions given in Table 1.

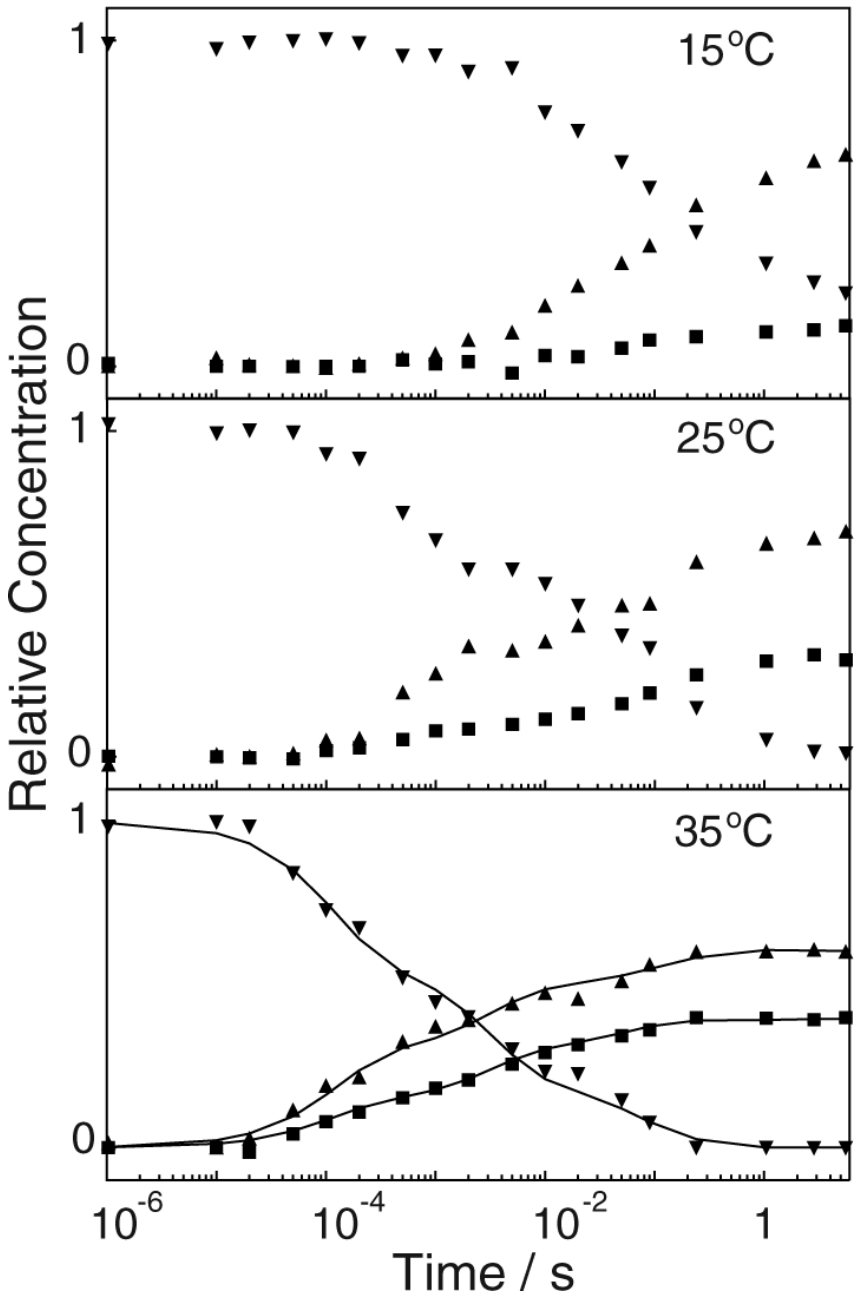

Figure 7.

Normalized temporal concentration profiles obtained by fitting photointermediate spectra to the raw data from crystal suspensions. Concentration profiles of photointermediates are normally determined using the microscopic rate constants describing the mechanism that best fits the data. In the case of rhodopsin 2D crystals, no single mechanism could be found to fit the data, and these concentration profiles shown by the plotted points (Lumi, ▼; Meta I_{480}, ▲; 380 nm absorbers Meta I_{380} and Meta II*(MII_a), ■) were determined by directly fitting the raw data to photointermediate spectra. As a consequence of the empirical nature of the fit, the 380 nm absorbing product cannot be differentiated into Meta I_{380} and Meta II*(MII_a). The continuous change seen in these concentration curves, as opposed to the temporally localized changes expected when exponentials describe the underlying processes, documents the

difficulty encountered in fitting a single mechanism with discrete exponentials. The continuous curves in the 35 °C panel show the concentration profiles produced by the more complex, heterogeneous mechanism described in the text.

Table 1

Decomposition of b-spectra in terms of photointermediates

15 °C	**b_1**	**b_2**	**b_3**	**b_0**
Lumi (494 nm)	0.26	0.55	*a*	0.2
Meta I_{480} (484 nm)	−0.23	−0.46	*a*	0.69
Meta I_{380} or II* (384 nm)	−0.03	−0.09	*a*	0.1
bleach (508 nm)	0	0	*a*	−1
25 °C				
Lumi (494 nm)	0.45	0.57	*a*	0
Meta I_{480} (484 nm)	−0.35	−0.36	*a*	0.71
Meta I_{380} or II* (384 nm)	−0.09	−0.18	*a*	0.26
bleach (508 nm)	0	0	*a*	−1
35 °C				
Lumi (494 nm)	0.51	0.2	0.3	0
Meta I_{480} (484 nm)	−0.35	−0.05	−0.19	0.6
Meta I_{380} or II* (384 nm)	−0.15	−0.16	−0.06	0.34
NRO (420 nm)	0	0	−0.04	0.04
bleach (508 nm)	0	0	0	−1

a At this temperature only two time dependent b-spectra were fit to the data.

Table 2

Microscopic rate constants for heterogeneous rhodopsin crystal schemes at 35 °C

	fast (28%)	membrane-like (50%)	slow (22%)
k_1 Lumi → Meta I_{380}	*a*	2,500 s^{-1}	8 s^{-1}
k_2 Meta I_{380} → Lumi	*a*	6,000 s^{-1}	4 s^{-1}
k_3 Meta I_{380} → Meta I_{480}	*a*	650 s^{-1}	4 s^{-1}
k_4 Lumi → Meta I_{480}	8,000 s^{-1}	170 s^{-1}	5 s^{-1}
k_5 Meta I_{480} → Meta II*(MII_a)	*a*	4 s^{-1}	0.4 s^{-1}
k_6 Meta II*(MII_a) → Meta I_{480}	*a*	3 s^{-1}	0.4 s^{-1}

*a*This subscheme contains only one step.